

Article

Investigation of Reasonable Reserved Deformation of Deep-Buried Tunnel Excavation Based on Large Deformation Characteristics in Soft Rock

Zhen Yang ¹, Peisi Liu ², Bo Wang ³, Yiqi Zhao ³ and Heng Zhang ^{3,*}¹ Gansu Tianlong Railway Co., Ltd., Lanzhou 730020, China; yzhen_2024@outlook.com² China Railway Eryuan Engineering Group Co., Ltd., Chengdu 610031, China; peisi_l@outlook.com³ Key Laboratory of Transportation Tunnel Engineering, Ministry of Education, Southwest Jiaotong University, Chengdu 610031, China; wb2023200105@my.swjtu.edu.cn (B.W.); zhaoyiqi2022200052@my.swjtu.edu.cn (Y.Z.)

* Correspondence: tunnelzh@home.swjtu.edu.cn; Tel.: +86-028-87634386

Abstract: This study studies the deformation characteristics of the diversion tunnel of Jinping II Hydropower Station in order to guarantee the safety of the excavation of a large-section soft rock tunnel with a depth of 1000 m and increased ground stress. Using field data, theoretical computations, and numerical modeling, the proper reserved deformation of a deep soft rock tunnel is investigated, taking into consideration the size, in situ stress, and grade of the surrounding rock. The study reveals that (1) The diversion tunnel's incursion limit, which is typically between 20 and 60 cm, is serious; (2) The surrounding rock level > geostress > tunnel size are the influencing parameters of reserved deformation that remain unchanged while using the numerical simulation method, which is more accurate in simulating field conditions; (3) The west end of the Jinping diversion tunnel has a 30–60 cm reserved deformation range for the chlorite schist tunnel. The deformation law of a large-section, 1000 m-deep soft rock tunnel is better understood, and it also offers important references for high-stress soft rock tunnel engineering design, construction, and safety management.

Keywords: tunnel; reserved deformation; high in situ stress; large deformation; influencing factors



Citation: Yang, Z.; Liu, P.; Wang, B.; Zhao, Y.; Zhang, H. Investigation of Reasonable Reserved Deformation of Deep-Buried Tunnel Excavation Based on Large Deformation Characteristics in Soft Rock. *Buildings* **2024**, *14*, 3159. <https://doi.org/10.3390/buildings14103159>

Academic Editor: Hugo Rodrigues

Received: 15 August 2024

Revised: 20 September 2024

Accepted: 27 September 2024

Published: 3 October 2024



Copyright: © 2024 by the authors. Licensee MDPI, Basel, Switzerland. This article is an open access article distributed under the terms and conditions of the Creative Commons Attribution (CC BY) license (<https://creativecommons.org/licenses/by/4.0/>).

1. Introduction

The tunnel construction was prone to rockburst [1–3], large deformation [4–6], and other diseases under the condition of deep-buried depth and high tectonic stress. Large deformation of tunnels in the case of soft rock and high in situ stress was more common than rockburst. The large deformation of the tunnel would aggravate the instability of the surrounding rock and bring about the distortion of the steel frame, the cracking of the initial support, the invasion limit, the loss and cracking of the secondary lining, the inverted arch uplift, and other related diseases [7,8], which would seriously affect the construction safety and progress and bring great risks to the construction of the tunnel. To control large deformation disasters, strengthening pre-supporting, improving support rigidity, adopting double-layer initial support, grouting reinforcement, and closing and forming a ring as soon as possible were the commonly used methods [9–11]. These methods had achieved good results in many cases. Based on the deformation characteristics of the surrounding rock, Zhang et al. [12] studied the reasonable tunnel shape of the high in situ stress and steeply inclined surrounding rock and believed that the optimization of the cavity type could fundamentally reduce the stress and deformation of the tunnel structure. Xu et al. [13] applied theories and tests to propose a steel grid concrete core tube support system, which could improve the support quality and prevent large deformation in tunnels. Qiu et al. [14] optimized the grille steel frame through element tests and refined the model calculation. This result did not significantly increase the number of steel bars but increased the bearing capacity of the initial support, which could effectively resist the deformation

of the tunnel. For tunnels with huge deformations, Wang et al. [15] applied high-stiffness steel tube concrete as the initial support to resist the deformation of the surrounding rock, which achieved good results. In addition to the large-rigidity support method for resisting the deformation, Qiu et al. [16] invented the resistance limiter for the initial support of the tunnel by using different stiffnesses between the materials. In addition to the large-rigidity support method for resisting the deformation, Qiu et al. [16] invented the support resistant limiting damper (SRLD) for the initial support by using the different stiffnesses between the materials. SRLD controlled the deformation by first letting down and then resisting, which had been used in the Menghua Railway. Various types of anchors had also been used in tunnels, such as NRP anchors [17], high constant resistance anchor cables [18], prestressed anchors (anchor cables) [17], etc. These absorbed the stress release caused by tunnel excavation in the surrounding rock and had a good effect in high in situ stress tunnels. In addition to the need for reasonable support parameters and construction methods, it was of great significance to grasp the deformation characteristics of the tunnel and select a reasonable amount of reserved deformation [19–22].

The current “Specifications for Design of Highway Tunnels Section 1 Civil Engineering” (JTG3370.1-2018) [23] and “Code for Design of Railway Tunnels” (TB 10003-2016) [24] both had instructions for the reserved deformation for the classification of surrounding rock. They were the main basis for the design of the reserved deformation of Chinese tunnels. Meanwhile, based on the deformation field survey and on-site monitoring and measurement data of the Lianchengshan tunnel, Chen et al. [19] statistically analyzed the deformation of the tunnel under different chlorite schist rock mass conditions, studied the deformation law, and reasonably reserved the amount of deformation. Deformation control benchmarks for deep-buried and large-span chlorite schist tunnel construction were established. For different rock mass states, four different reserved deformations of 70–95 cm, 50–70 cm, 30–50 cm, and 15–30 cm were given. Liu et al. [25] monitored a total of 471 sections in 14 tunnels of the Yuchu Expressway. He used the interval statistical method to calculate the reserved deformation of tunnels at different levels of surrounding rock and at different buried depths. It is recommended that when the buried depth of Grade IV surrounding rock is less than 50 m, the reserved deformation is set to 17 cm. It is recommended that when the buried depth is 50–300 m, the reserved deformation is set to 50 cm. It is recommended that when the buried depth of Grade V surrounding rock is less than 50 m, the reserved deformation is set to 18 cm. It is recommended that when the buried depth is 50–300 m, the reserved deformation is set to 32 cm. Zhao et al. [26] proposed a method of optimizing the reserved deformation based on the whole-section analysis and on the 3D laser scanning technology. The step-like method of setting aside the amount of deformation was adopted (the dome was 7 cm, and the rest area was 5 cm). Li et al. [27] used the theory of elastoplastic mechanics to derive the analytical solutions of the surrounding stress and displacement at different stages and the radius of the crack and plastic zone. In response to the problems in a tunnel in Xuzhou, 20 cm reserved deformation layers were proposed. Luo et al. [28] analyzed the stress and deformation characteristics of the tunnel, using numerical calculation software, and obtained the reserved deformation of the loess tunnel with different moisture contents. Cui et al. [29] determined the asymmetric reserved deformation value of the loess tunnel through the method of a model test and believed that the reserved deformation of the vault should be two to four times that of the sidewall. Wang et al. [30] gave the respective reserved deformations under the three conditions of hard plastic, soft plastic, and flow plastic for large-section double-track loess tunnels. They were hard plastic (vault 55–70 mm, sidewall 15–20 mm), soft plastic (vault 166–180 mm, sidewall 40–50 mm), and flow plastic (vault 290–300 mm, sidewall 125–140 mm).

Many scholars have carried out in-depth research on the reserved deformation in tunnel construction and put forward the corresponding reasonable reserved deformation according to different soft rock geological conditions. These research results are mainly related to the strength of the surrounding rock, buried depth (i.e., geostress level), and other key factors. For soil tunnels, especially loess tunnels, the distribution of reserved

deformation is obviously uneven, and the important variable of water content should be additionally considered. However, at present, most of the research on reserved deformation focuses on tunnels with buried depths less than 500 m. With the development of tunnel engineering technology to a deeper level, especially for tunnels with a depth of 1000 m, the in situ stress level is much higher than that of conventional tunnels, which makes the prediction and control of tunnel deformation more complicated and arduous. Under such extreme conditions, how to determine the reserved deformation scientifically and reasonably to ensure the stability and safety of the tunnel structure has become a technical problem to be solved urgently. In addition, for tunnels with a large cross-section, high ground stress, soft rock, and other special working conditions, the current design specifications often lack specific guidance on reserved deformation, which further increases the construction difficulty and risk. Therefore, future research should focus on the reserved deformation law of tunnels under these complex conditions and explore more accurate and reliable prediction and control methods of reserved deformation through theoretical analysis, numerical simulation, field tests, and other means so as to provide strong support for the safe and efficient construction of tunnel projects. In this paper, the deformation characteristics of a diversion tunnel of Jinping II Hydropower Station are studied. Based on field statistics, theoretical calculation, and numerical simulation, and considering the size, in situ stress, and grade of the surrounding rock, the reasonable reserved deformation of the deep soft rock tunnel is studied.

2. Project Overview and Geological Conditions

The Jinping II Hydropower Station is located on the Jinping River Bay, the mainstream of the Yalong River in Sichuan Province. It was the largest hydropower station in the cascade development of the Yalong River and one of the backbone power stations for power transmission from west to east. The terrain along the tunnel is undulating. The height of the mountain at the western end of the tunnel entrance is about 500 m, and then the buried depth gradually increases. The project location and cave entrance photos are shown in Figure 1. The diversion system of Jinping II Hydropower Station is meticulously built, including Jinping auxiliary tunnel lines A and B, four diversion tunnels, and drainage tunnels, for a total of seven major tunnels placed in parallel, as illustrated in Figure 2a. The Jinping auxiliary tunnel was built using efficient drilling and blasting techniques, and its standard section was planned as a distinctive gate-shaped section with an excavation area of 45 m². The horseshoe-shaped section facing the emergency stop area has been adjusted for safety, and the excavation area has been increased to 55 m². The drilling and blasting process and advanced tunnel boring machine (TBM) technology are used in a unique way to construct a diversion tunnel. For the section excavated by drilling and blasting, advanced bench construction technology was used, resulting in a horseshoe-shaped section with an excavation diameter of 13 m and an upper excavation area of 110 m², significantly improving the construction efficiency and quality. To address the project's water inrush issue and ensure the smooth construction of the diversion tunnel, the project team expertly built a critical drainage tunnel between auxiliary tunnel B and diversion tunnel 4. This drainage tunnel fully utilizes the full-face TBM excavation technology. The excavation diameter is precisely controlled at 7.2 m, and the excavation area is efficiently maintained at 41 m², ensuring effective water flow management and material transportation during the construction period while demonstrating the superior engineering design and construction level.

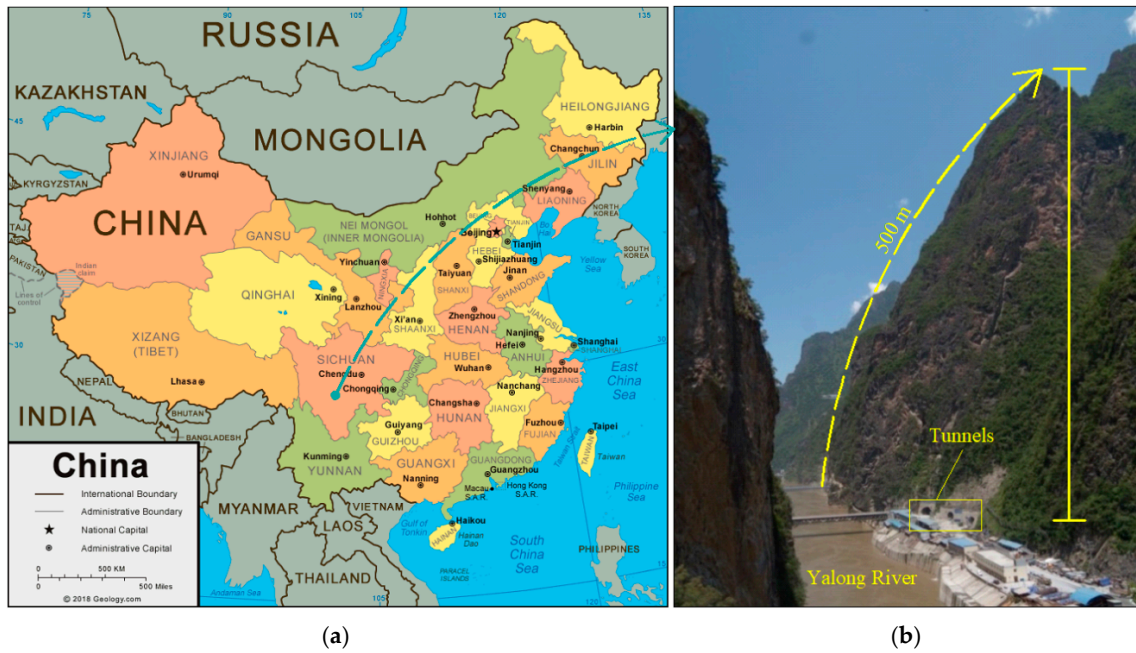


Figure 1. Schematic diagram of the project location and cave entrance. (a) Project location; (b) Schematic diagram of cave entrance.

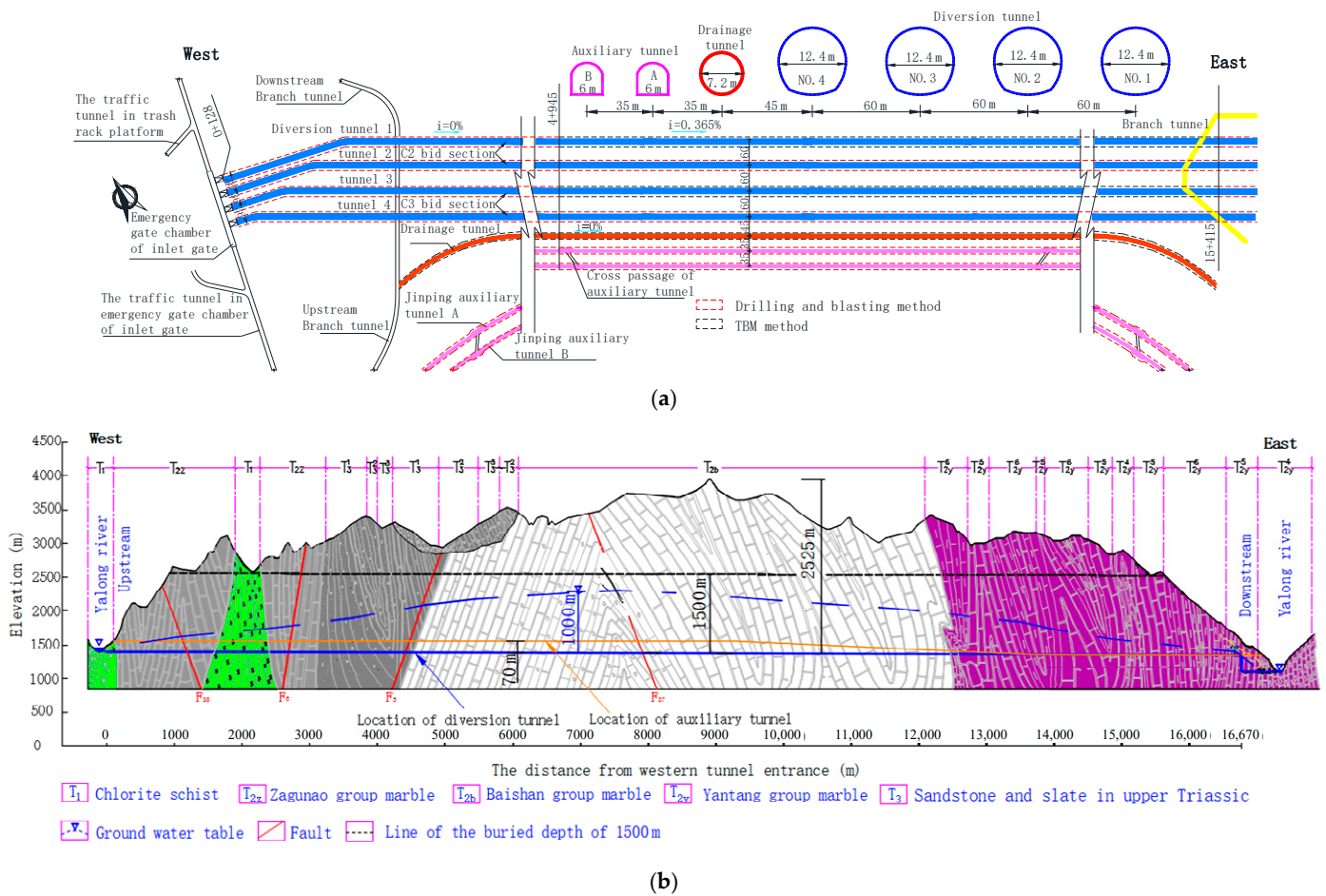


Figure 2. Layout and geologic condition of the Jinping II Hydropower Station. (a) Plane layout; (b) Engineering geologic profile.

The Jinping II Hydropower Station was affected by the collision of the Eurasian plate and the Indian Ocean plate and mainly composed of middle and upper Triassic marble, limestone, crystalline limestone and sandstone, and slate. The diversion tunnel also includes lower Triassic green sandstone and chlorite schist. From east to west, the tunnels passed through various strata including marble of the Yantang (T_{2y}) group, marble of the Baishan group (T_{2b}), upper Triassic (T_3) marble, marble of the Zagunao group, lower Triassic (T_1) chlorite schist, and metamorphic medium-to-fine sandstone, as shown in Figure 2b. According to the tectonic history and orientation, the faults in the project area could be divided into four structural groups in the NNE direction, NNW direction, NE-NEE direction, and NW-NWW direction (all have a steep inclined angle), respectively. The surrounding rock is dominated by class II and III (hydraulic classification), and class IV and V account for about 23% to 30%, mainly concentrated in the T_1 strata. The buried depth of tunnels was generally 1500–2000 m, with the maximum buried depth being 2525 m. The maximum in situ stress in the engineering area is 80 MPa, the uniaxial compressive strength of chlorite schist is 19.47 to 38.80 MPa, and the strength–stress ratio of the surrounding rock is 0.24 to 0.49, which has strong and extremely strong large deformation conditions. The prediction and prevention of large deformation is the key to ensuring construction safety.

3. Mechanical Properties of Chlorite Schist

3.1. Rock Strength

The mechanical properties test of chlorite schist was carried out with a rock mechanics rigidity testing machine, as shown in Figure 3. The test adopted displacement control, with the loading rate being 0.002 mm/s. The 5 mm displacement sensor was used to test the axial displacement of the sample. The 1000 kN force sensor was used to test the axial load of the sample. The loading method of the instrument was uniform load, with the maximum axial force as 1000 kN and the maximum confining pressure as 50 MPa.

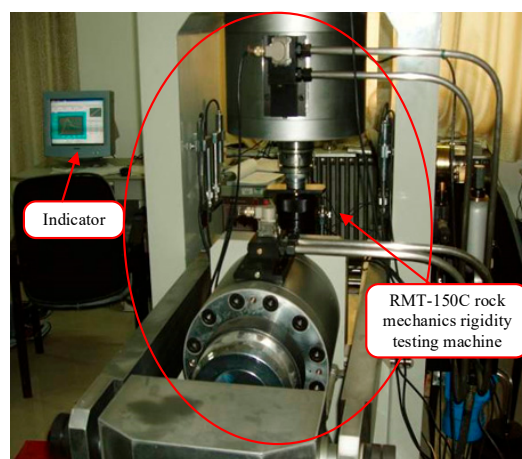


Figure 3. Test equipment.

The specimens were obtained from the exposed chlorite schist section at the west end of the Jinping secondary diversion tunnel. The collected mileages were Tunnel 1 1 + 550, Tunnel 1 1 + 650, Tunnel 2 1 + 620, and Tunnel 2 1 + 640. The chlorite schist in this area was black-green to gray-green, weak to slightly weathered, fine in texture, and slightly slippery and had no obvious flakes. The overall continuity and integrity are relatively good. The sample preparation was required to be processed in strict accordance with the International Society of Rock Mechanics (ISRM) test regulations, as shown in Figure 4.

First, the sample was wrapped up in latex sleeves to prevent hydraulic oil from intruding into the specimen during the test, affecting the determination of the rock mechanics characteristic parameters. Second, rigid spacers matching the diameter of the sample were added at both ends to reduce the impact of end face friction on the test results. Then, the sample was put into the triaxial pressure chamber with a predetermined confining pressure.

The specimen was under hydrostatic pressure at this point. Eventually, the sample was subjected to axial stress, which caused it to fracture and lose its ability to support weight.



Figure 4. The specimen.

When the confining pressure was low, the stress reduction value was higher. As the confining pressure increases, the stress reduction value became smaller and tended to the ideal elastoplastic deformation behavior, as shown in Figure 5. The mechanical properties of chlorite schist were sensitive to confining pressure. Under dry and saturated conditions, the relationship between the peak strength and the confining pressure is shown in Figure 6, which was in line with the linear characteristics of the Mohr–Coulomb strength criterion. Chlorite schist under dry conditions was as follows: cohesion $c = 13.74$ MPa, friction $\Phi = 21.43^\circ$. Under saturated conditions, its cohesion $c = 4.47$ MPa and its friction $\Phi = 25.26^\circ$.

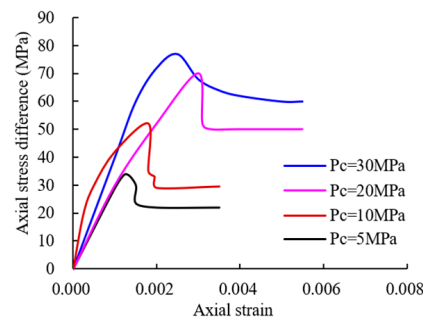


Figure 5. Stress–strain curves.

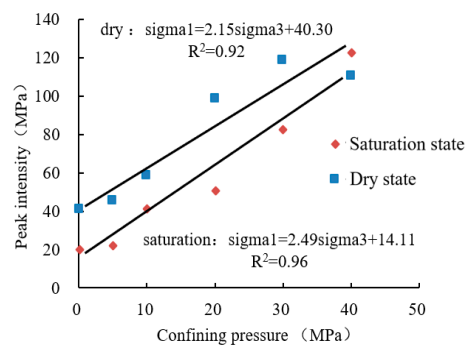


Figure 6. Relationship between peak intensity and confining pressure.

Figure 7 displays the chlorite schist test failure forms under triaxial compression. The test results demonstrated that shear failure was the cause of the samples' failure at various confining pressure settings. The specimen was a macroscopic single-section shear failure

at decreased confining pressure. The rock specimen's macroscopically observed fracture revealed a comparatively rough fracture surface. Numerous tiny fragments started to show up close to the fracture surface at the same moment. The specimens would likewise appear near to parallel double-section shear failure with a rise in confining pressure. Strong friction on the shear fracture surface created white powder, and the fracture surface was flatter than it had been previously.

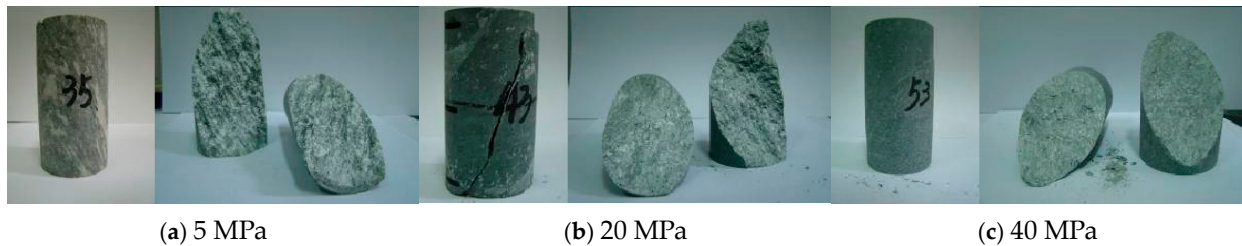


Figure 7. Failure mode under triaxial compression.

3.2. Rock Mass Parameter Conversion

The mature 2002 Hoek–Brown [31,32] strength criterion is adopted to convert the rock mass strength index. The calculation formula is as follows:

$$\sigma_1 = \sigma_3 + \sigma_c \left(\frac{m_b}{\sigma_c} \sigma_3 + s \right)^a \quad (1)$$

where σ_1 is the maximum principal stress when the rock mass fails σ_3 is the minimum principal stress when the rock mass fails, σ_c is the rock uniaxial compressive strength, m_b/s is the Hoek–Brown criterion empirical parameters, and a is the coefficient determined by the characteristics of the rock mass.

$$m_b = m_i \exp\left(\frac{GSI - 100}{28 - 14D}\right) \quad (2)$$

$$s = \exp\left(\frac{GSI - 100}{9 - 3D}\right) \quad (3)$$

$$a = \frac{1}{2} + \frac{1}{6} \left(e^{-GSI/15} - e^{-20/3} \right) \quad (4)$$

where m_i is the lithology index, D is the disturbance factor, and GSI is the geological strength index of the rock mass.

$$E_m = \begin{cases} \left(1 - \frac{D}{2}\right) \sqrt{\frac{\sigma_c}{100}} 10^{\left(\frac{GSI-10}{40}\right)}, & (\sigma_c \leq 100 \text{ MPa}); \\ \left(1 - \frac{D}{2}\right) 10^{\left(\frac{GSI-10}{40}\right)}, & (\sigma_c \geq 100 \text{ MPa}). \end{cases} \quad (5)$$

where E_m is the rock elastic modulus and m_i is the Hoek–Brown constant of the intact rock block.

$$D = 1 - K_v \quad (6)$$

where K_v is the rock mass integrity index. The calculation formula is

$$K_v = \left(\frac{V_{pm}}{V_{pr}} \right)^2 \quad (7)$$

where K_v is the rock mass integrity index, V_{pm} is the longitudinal wave velocity of the rock mass, and V_{pr} is the longitudinal wave speed of indoor rock.

$$GSI = 15V_{pm} - 7.5 \quad (8)$$

Regarding the method of determining the secant strength of the M-C strength criterion, Hoek updated the Formula (9) conversion relationship:

$$\varphi = \sin^{-1} \left[\frac{6am_b(s + m_b\sigma_{3n})^{a-1}}{2(1+a)(2+a) + 6am_b(s + m_b\sigma_{3n})^{a-1}} \right]$$

$$c = \frac{\sigma_c[(1+2a)s + (1-a)m_b\sigma_{3n}] + (s + m_b\sigma_{3n})^{a-1}}{(1+a)(2+a)\sqrt{1 + (6am_b(s + m_b\sigma_{3n})^{a-1}) / (1+a)(2+a)}} \quad (9)$$

where $\sigma_{3\max}$ is Formula (10) for calculation.

$$\frac{\sigma_{3\max}}{\sigma_{cm}} = 0.47 \left(\frac{\sigma_{cm}}{\gamma H} \right) \quad (10)$$

where H is the tunnel buried depth, γ is the rock mass, and σ_{cm} is the uniaxial compressive strength of the rock mass defined by the H-B criterion, which is taken according to Formula (11).

$$\sigma_{cm} = \sigma_c \cdot \frac{(m_b + 4s - a(m_b - 8s))(m_b/4 + s)^{a-1}}{2(1+a)(2+a)} \quad (11)$$

It was confirmed by the literature [32] that the E_m , C , and φ calculated from related parameters such as GSI, D , and m_i are shown in Table 1. To facilitate subsequent calculations and achieve calculation accuracy at the same time, the reduced data had been retained to a certain degree.

Table 1. Mechanical parameters of surrounding rock.

Surrounding Rock Category	GSI	D	m_i	E_m (Gpa)	C (Mpa)	φ (°)
III	55	0.55	25	5.80	0.87	46.84
IV	40	0.60	20	2.89	0.59	36.60
V	28	0.80	17	1.07	0.32	25.41

4. Deformation Characteristics of Tunnel

4.1. Deformation Phenomenon

The overall deformation characteristics of the surrounding rock in the tunnel section (Tunnel 1 1 + 535 m~1 + 759 m, Tunnel 2 1 + 613 m~1 + 643 m) where the exposed chlorite schist was located could be reflected through the observation and analysis of the on-site construction situation. During the excavation of the upper section of the tunnel, the severe deformation of the surrounding rock caused by the rupture of the sprayed layer, the bulging of the surrounding rock, and the distortion of the arch frame reflect some of the characteristics of the overall deformation of the surrounding rock. The arches on both sides were the parts where the cross-section diseases are more concentrated. There was serious voiding of the concrete shotcrete at the arch foot on the north side of the Tunnel 1 1 + 660 m section, with the largest crack exceeding 20 cm. Vertical cracks with shear characteristics appeared in the lower part of the sidewall on the north side of the Tunnel 1 1 + 670 m section. The disease is shown in Figure 8. Except for the arch feet on both sides, there was no large-area concrete spraying damage at the other larger deformed parts. The cave wall uplift phenomenon was more common in the other parts.

A section scanner was used to measure the deformed sections after the west end diversion tunnel demonstrated that the T1 chlorite schist section's convergent deformation was stable. It was discovered that this tunnel section's "diameter reduction" phenomena was clearly visible, as seen in Figure 9.

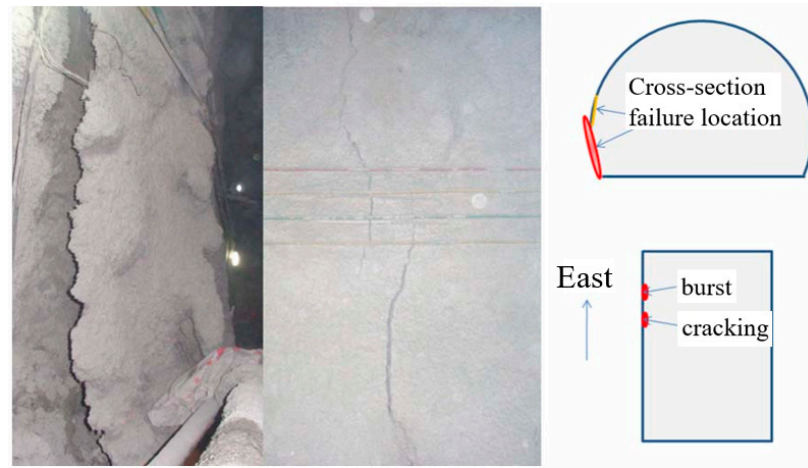


Figure 8. Spray layer opening, voiding, and cracking.

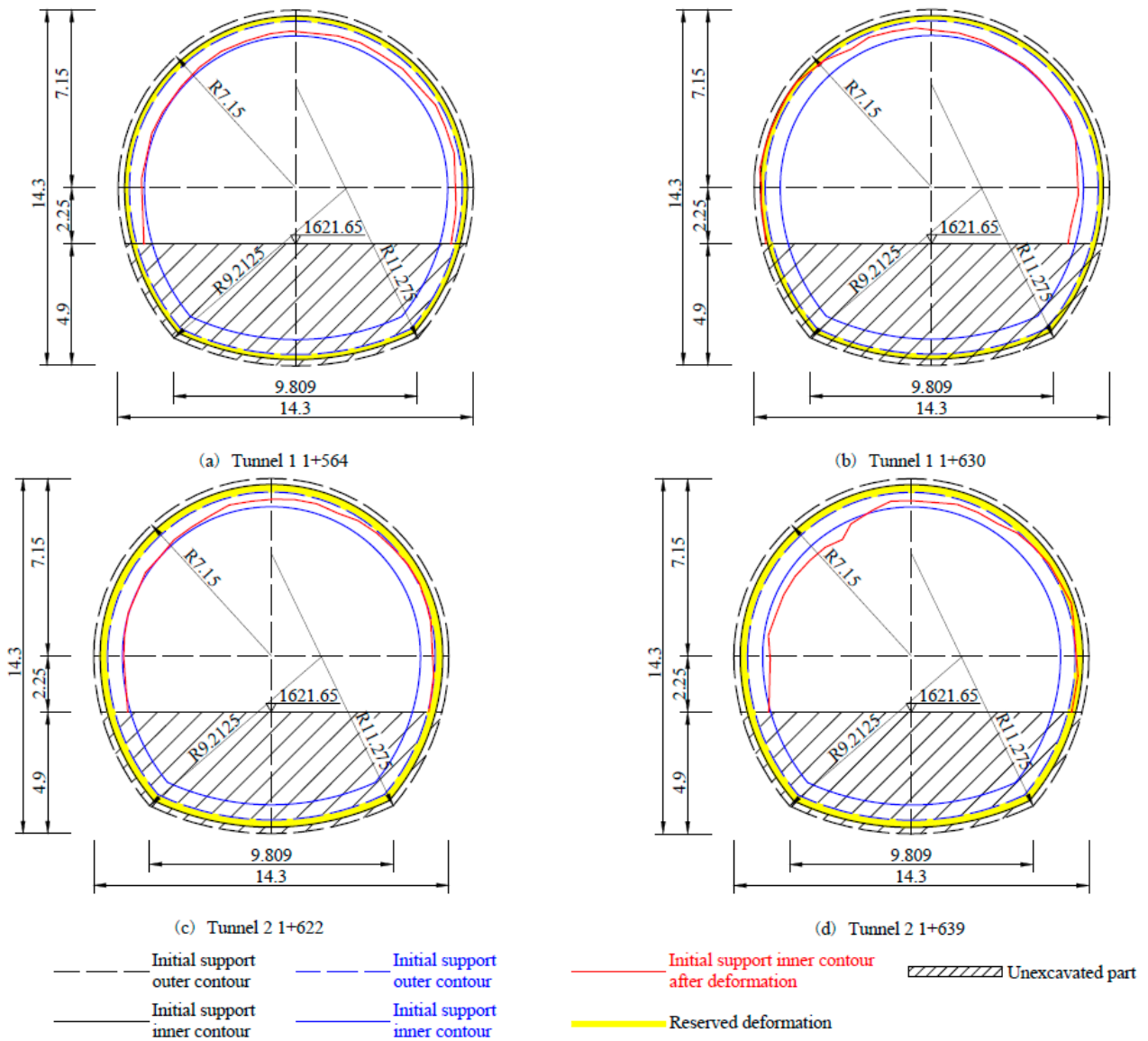


Figure 9. Deformation contour line of a typical section (Units: m).

According to statistics, the Tunnel 1 + 535~1 + 759 m section had 105 scanning sections, and the Tunnel 1 + 613~1 + 643 m section had 16 scanning sections. The histograms of the

maximum deformation of every section invading the lining clearance section are shown in Figure 10.

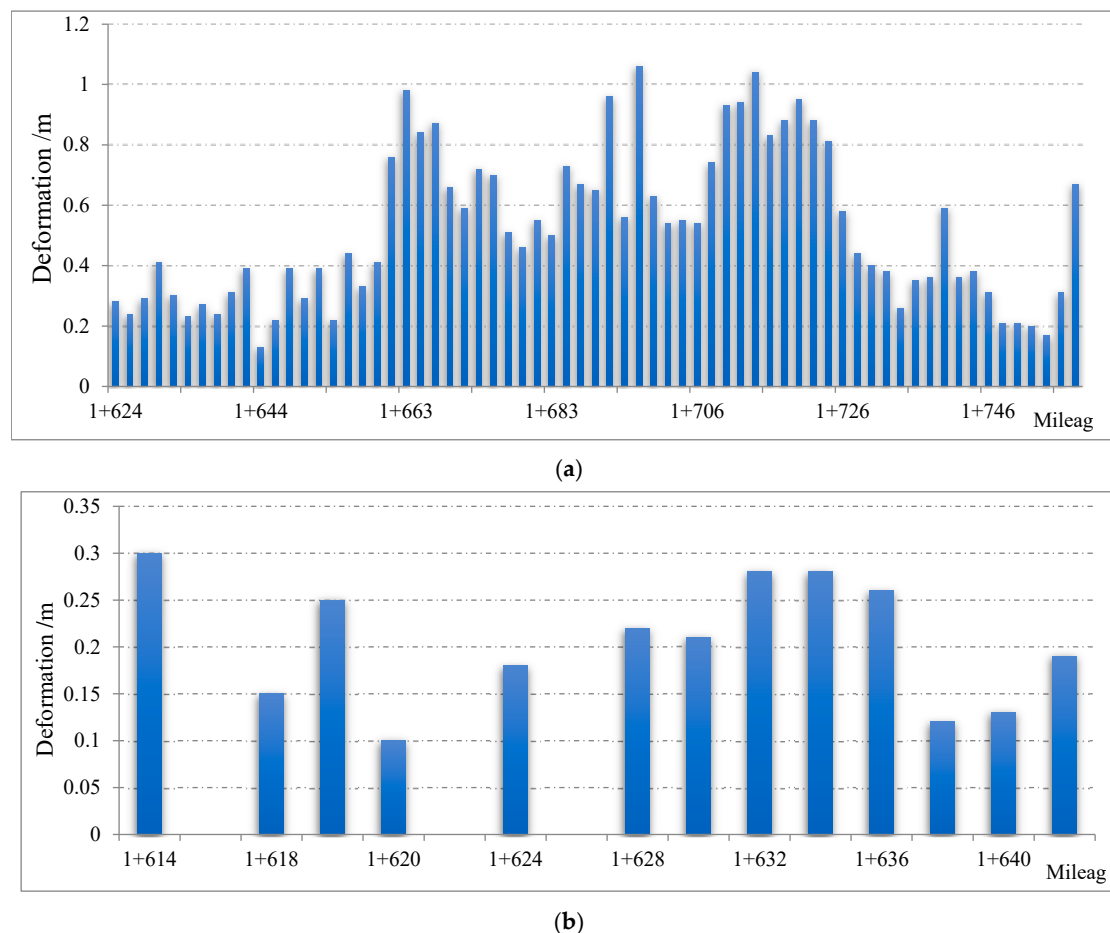


Figure 10. Tunnel intrusion limit statistics. (a) Tunnel 1 1 + 624~759 m; (b) Tunnel 2 1 + 613~1 + 643 m.

Through the summary of the measurement situation, it could be found that the tunnel deformation has the following characteristics:

The tunnel sections with severe deformation problems were mainly concentrated in pure chlorite schist sections, occupying 21.7~176.7% of the design lining space. The design lining clearance thickness invaded by surrounding rock deformation of the tunnel was generally more than 20 cm, mostly between 20 and 60 cm, and some were more than 1 m. The distribution law of the large deformation of Tunnel 1 and Tunnel 2 was generally close. Tunnel 1 was more inclined to the north sidewall, and the largest deformation of more cross-sections occurred on the south side of the arch foot. Tunnel 2 mainly occurred on the north side arch, and there was a large deformation from the arch toe to the top arch.

4.2. Deformation Characteristics

The surrounding rock deformation and stress redistribution during the tunnel construction process are constantly changing with the advancement of the tunnel face (space change), which is called the spatial effect (sometimes called the space-time effect). Compared with the plane issue, the existence of the tunnel face is restricted to a certain extent, and the degree of restriction is related to the specific distance from the tunnel face. The farther the distance from the tunnel face, the smaller the constraint. This characteristic is of great significance to the design of tunnel excavation and support.

The buried depth of the tunnel exceeded 1500 m, which could be regarded as a hydrostatic state, and the lateral pressure coefficient was 1.0. In this section, finite difference calculation software was used to simulate several main factors that affect the deformation of surrounding rock. The deformation characteristics of the surrounding rock of the tunnel under different burial depths, tunnel lengths, and strengths of the surrounding rock were analyzed, which provided a basis for the analysis of the reserved deformation of the Jinping diversion tunnel. According to different factors affecting the deformation of the surrounding rock, simulations of eleven working conditions were carried out, as shown in Table 2. The yield of the rock mass obeyed the Mohr–Coulomb criterion. At the same time, combined with the actual construction on site, the simulation analysis was mainly carried out on the excavation of the upper half section. The calculation model was taken from the green mud schist section of the tunnel, with a size of 120 m × 120 m × 60 m, as shown in Figure 11. The middle section in the z direction was taken as the monitoring section. Since the early strength of shotcrete cannot be controlled, the role of support was not considered here.

Table 2. Simulation conditions and parameters.

	Number	Surrounding Rock Category	Diameter (m)	In Situ Stress (MPa)	Density ρ (kg/m ³)	Poisson's ratio/ μ	Friction φ (°)	Cohesion c (MPa)	Elastic Modulus (GPa)
In situ stress	1	IV	13.4	10	2600	0.32	36.60	0.59	2.89
	2			20					
	3			30					
	4			40					
Tunnel size	5	IV	12	35	2600	0.32	36.60	0.59	2.89
	6		13						
	7		14						
	8		15						
Surrounding rock category	9	III	13.4	35	2700	0.27	46.84	0.87	5.80
	10	IV			2600	0.32	36.60	0.59	2.89
	11	V			2400	0.40	25.41	0.32	1.07

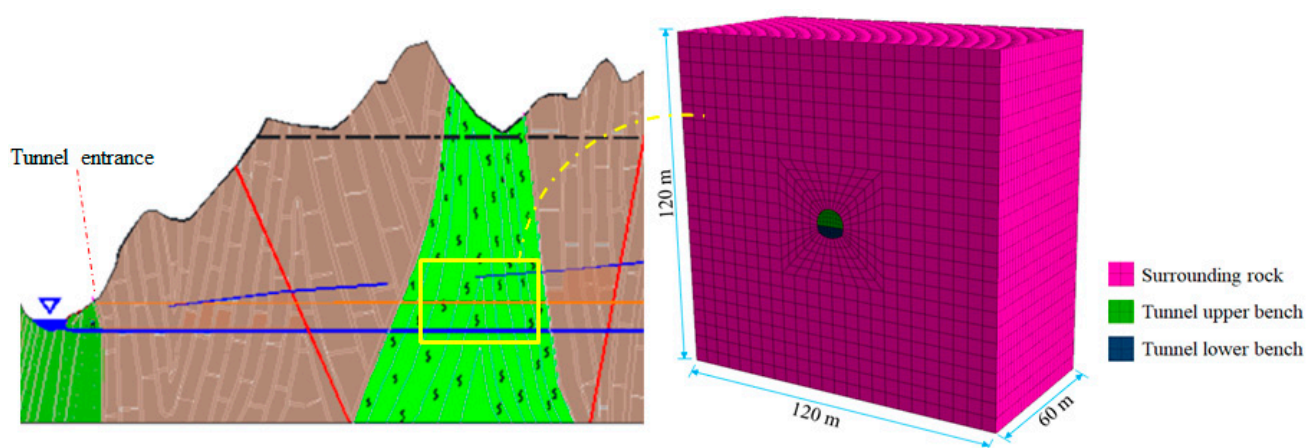


Figure 11. Calculation model.

The pattern of rock displacement around the rock under various in situ forces is depicted in Figure 12. It is evident that when the stress level in the tunnel's immediate vicinity surpasses the critical 20 MPa threshold, the displacement of the vault and arch waist will rise significantly, clearly surpassing other reasonably stable regions in the vicinity. The fragility and variability of the tunnel arch structure under a high-stress environment

are emphasized. Further, with the continuous increase in in situ stress, the deformation behavior of the surrounding rock presents more complex and significant changes. First off, the scope of deformation progressively widened from the original local area to encompass a larger surrounding rock area, suggesting that the total stability of the rock mass around the tunnel is significantly impacted by the rise in in situ stress. Second, the magnitude of deformation also increases significantly, that is, the displacement of surrounding rock increases sharply with the increase in in situ stress, which not only increases the burden of the tunnel supporting structure but also may pose a threat to the long-term stability of the tunnel. Therefore, in view of this phenomenon, we need to take more effective engineering measures to deal with the influence of a high-stress environment on the stability of tunnel's surrounding rock. The displacement nephogram of other working conditions is similar, so we will not go into the details here. The corresponding regular curve is shown in Figure 13.

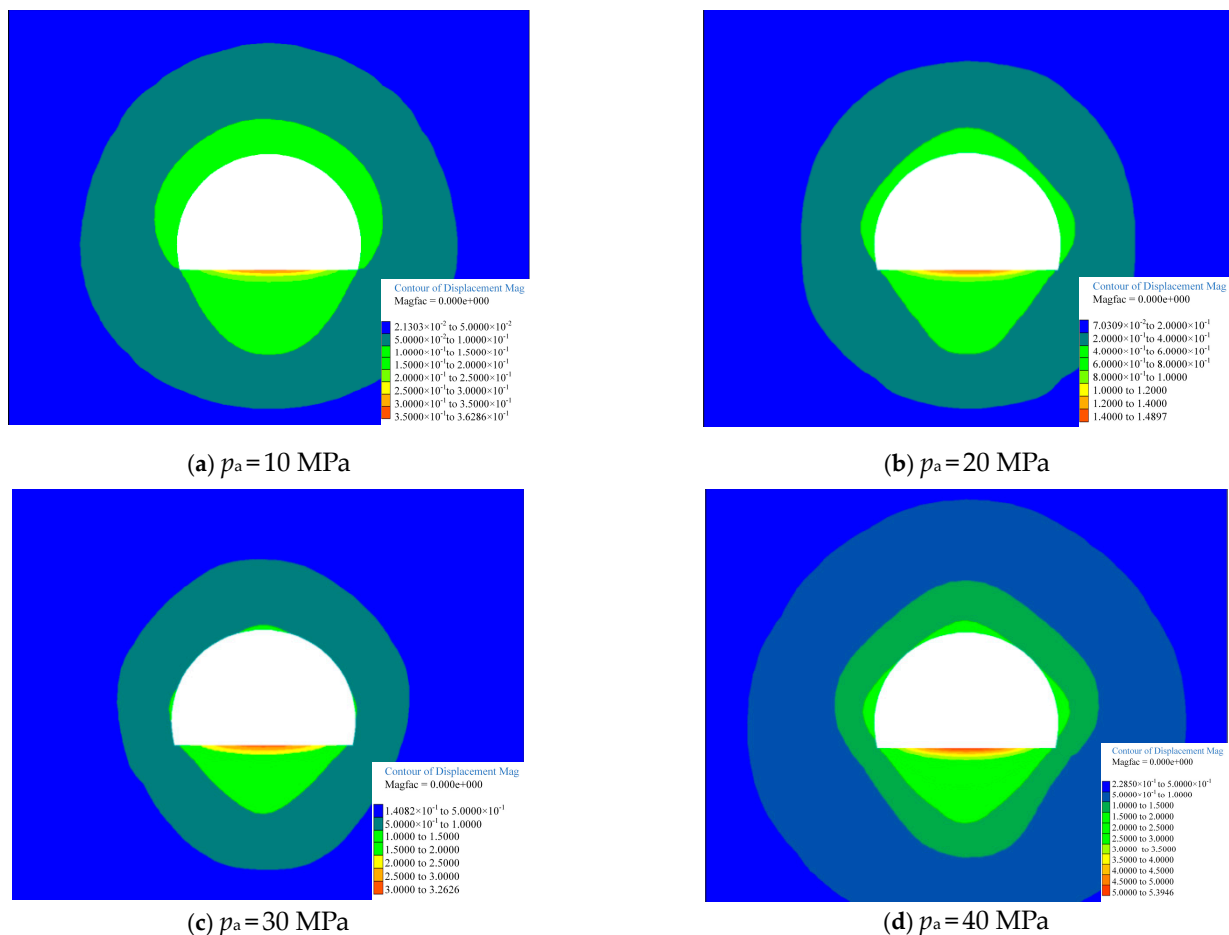


Figure 12. Cloud diagrams of different in situ stress and displacement distributions (p_a is in situ stress).

The vertical and horizontal deformation of the tunnel along with the in situ stress changes are shown in Figure 13a. With the increase in in situ stress, the settlement of the vault and the horizontal displacement of the vault gradually increased. The settlement increased from 15.77 cm in condition 1 to 169.2 cm in condition 4. The horizontal displacement increased from 14.42 cm to 175.55 cm. There was little difference between the settlement and horizontal convergence, which both increased linearly with the increase in in situ stress. Figure 13b showed the vertical and horizontal deformation curve with the hole diameter. The increase in the diameter of the hole led to a small increase in the amount of deformation. When the diameter of the hole increased by 1 m, the amount of deformation increased by about 5 cm. The deformation of the dome was slightly larger than

the deformation of the arch waist. The relationship between the level of the surrounding rock and the deformation of the tunnel is shown in Figure 13c. The values of the tunnel deformation of different levels of the surrounding rock vary greatly. When the level of the surrounding rock rises from level III to level V, the amount of deformation increases by about 100 times.

Through the analysis of the deformation characteristics of the tunnel, it was found that the deformation of the tunnel was related to the in situ stress, the diameter of the tunnel, and the level of the surrounding rock. The level of surrounding rock had the greatest impact, followed by the impact of in situ stress, and the size of the cavern had the least impact. The following research on the reserved deformation was also considered in terms of three aspects. Finally, the size of the reserved deformation was determined by relying on the actual parameters of the project.

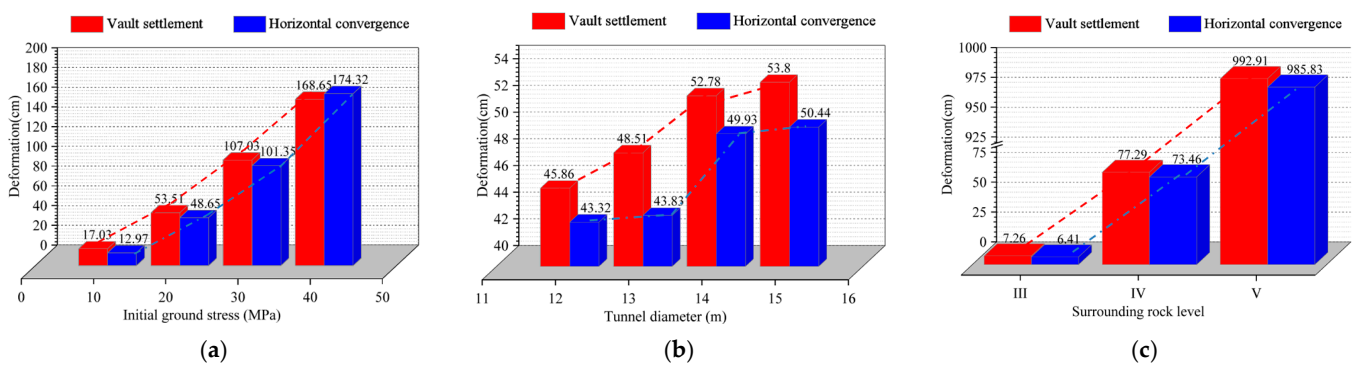


Figure 13. Deformation influencing factor relationship curve. (a) In situ stress; (b) Tunnel diameter; (c) Surrounding rock level.

5. Reserved Deformation

Because the initial support is closely attached to the surrounding rock, the local cracking and damage of the initial support will not cause the collapse of the entire tunnel. With the increase in the support displacement, the surrounding rock exhibits plastic deformation behavior, which is accompanied by the increase in and development of damage. When the damage develops to a certain extent, the initial support will not play the role of support. This is the excessive destruction of the initial support, and the stable state where the initial support and the surrounding rock deform together is the limit state of the initial support system.

5.1. Real Data Statistics

According to the statistics of the cross-sectional scan data of the deformed tunnel section (Tunnel 1 + 536~759 and Tunnel 2 + 613~643), when different reserved deformations were given, the corresponding guarantee rate relationship was as shown in Figure 13 and Table 3.

Table 3. Correspondence between the reserved deformation of the surrounding rock and the guarantee rate.

Reserved deformation (cm)		100	90	80	70	60	50	40	30
Guarantee rate (%)	Tunnel 1	98.10	93.33	87.62	83.81	78.10	67.62	59.05	35.24
	Tunnel 2	-	-	-	-	-	-	100	99

Figure 14a shows the statistics of the section scanning data of Tunnel 1. When the design reserved deformation was 40 cm, 50 cm, and 60 cm, the guarantee rates were 59.05%, 67.62%, and 78.01%, respectively. The guarantee rates were the probability that there would be no deformation greater than the reserved deformation amount. It could be seen that

the intrusion limit in the range of 1 + 660~720 m was significantly larger (generally above 60 cm), and the intrusion limit in other parts of the cave was about 40 cm. Tunnel 1's design may have a limited deformation range of 50–60 cm due to discrete on-site measurement data and a higher guarantee rate. Figure 14b shows the statistics of the section scanning data of Tunnel 2. When the design reserved deformation was 40 cm, the guarantee rate reached 100%. Tunnel 1 and Tunnel 2 were parallel and separated by 60 m, whose stratum lithology and in situ stress were comparable. Based on statistical data, Tunnel 2's reserved deformation may be compared to that of Tunnel 1, and a thorough examination may reveal that Tunnel 2's design reserved deformation range was between 30 and 40 cm.

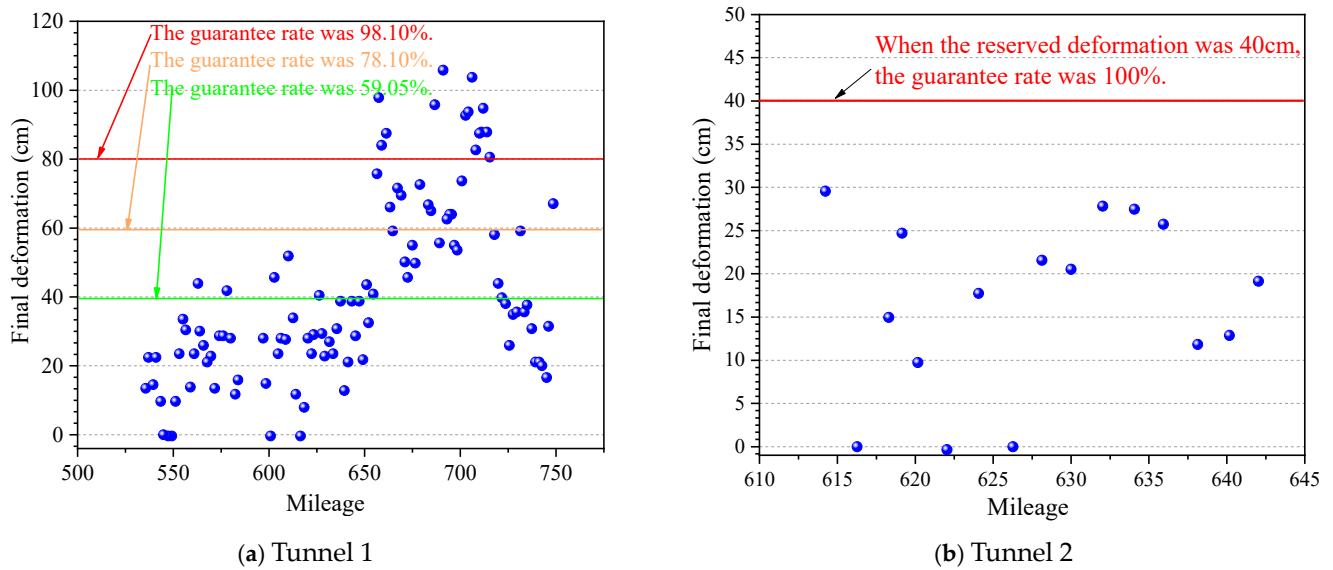


Figure 14. Correspondence between reserved deformation and guarantee rate.

5.2. Analytical Method

Within a deeply underground tunnel, a portion of the rock mass may transition into a plastic state due to either the local shear stress exceeding the shear strength of the rock mass or the secondary stress state of the surrounding rock exceeding the compressive strength of the surrounding rock. The Jinping diversion tunnel's substantial buried depth led to the assumption that the lateral pressure coefficient was 1. The ultimate displacement around the tunnel for three different p_a values (p_a is in situ stress)—0, 1, and 2 MPa—was examined using the elastoplastic method.

$$u_{r_0max}^p = \frac{R_0^2(1 + \mu)}{Er_0}(\sigma_Z - \sigma_{R_0}) \quad (12)$$

where $u_{r_0max}^p$ is the displacement around the tunnel (m), μ is Poisson's ratio, E is the elastic Modulus (MPa), σ_Z is the initial in situ stress (MPa), r_0 is the tunnel radius (m), R_0 is the plastic zone radius (m), and σ_{R_0} is the radial stress on the boundary of the plastic zone.

The radius of the plastic zone (R_0) was calculated using the following formula:

$$R_0 = r_0 \left[(1 - \sin\varphi) \frac{cco\varphi + \sigma_Z}{ccot\varphi + p_a} \right]^{\frac{1 - \sin\varphi}{2\sin\varphi}} \quad (13)$$

where c is the cohesion (MPa), φ is the friction ($^\circ$), and p_a is the supporting reaction force (MPa).

The radial stress σ_{R_0} on the boundary of the plastic zone is calculated using the following formula:

$$\sigma_{R_0} = \sigma_Z(1 - \sin\varphi) - cco \quad (14)$$

The parameters in Table 2 were used to calculate the displacement around the tunnel when the supporting resistance p_a is 0 MPa, 1 MPa, and 2 MPa under different in situ stress conditions under Type III and IV surrounding rocks. Figure 15 showed the relationship between the displacement of the unsupported tunnel and the initial stress. Figures 16 and 17 are the curves when the supporting reaction force was 1 MPa and 2 MPa.

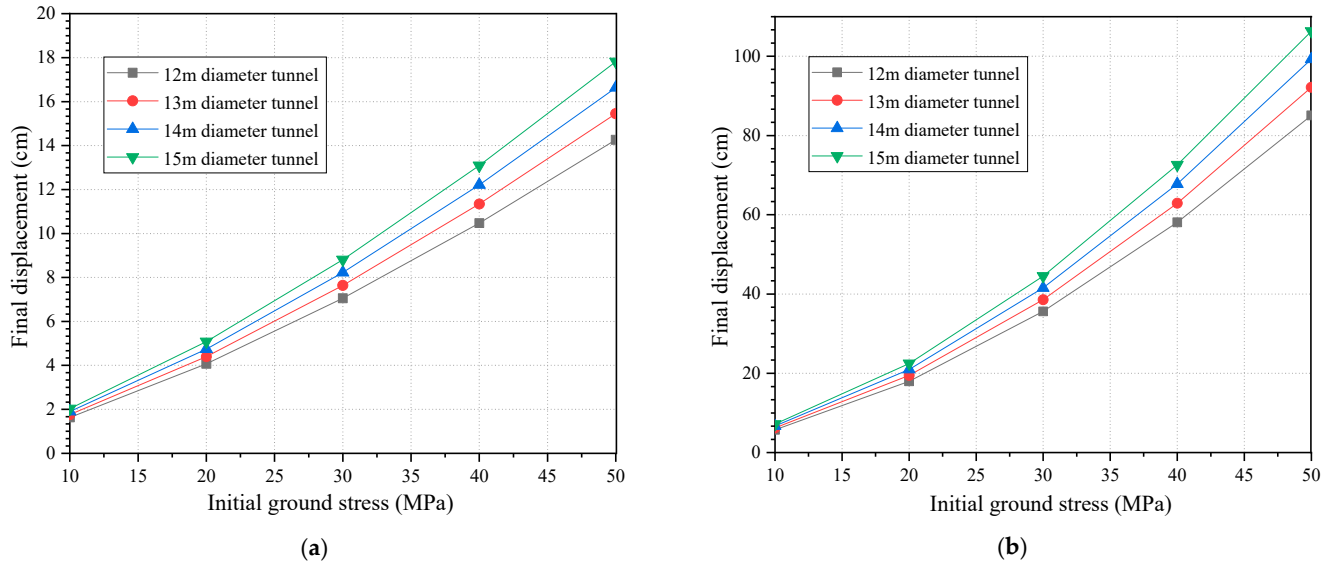


Figure 15. Final displacement curve around unsupported tunnel ($p_a = 0$ MPa). (a) Type III surrounding rock; (b) Type IV surrounding rock.

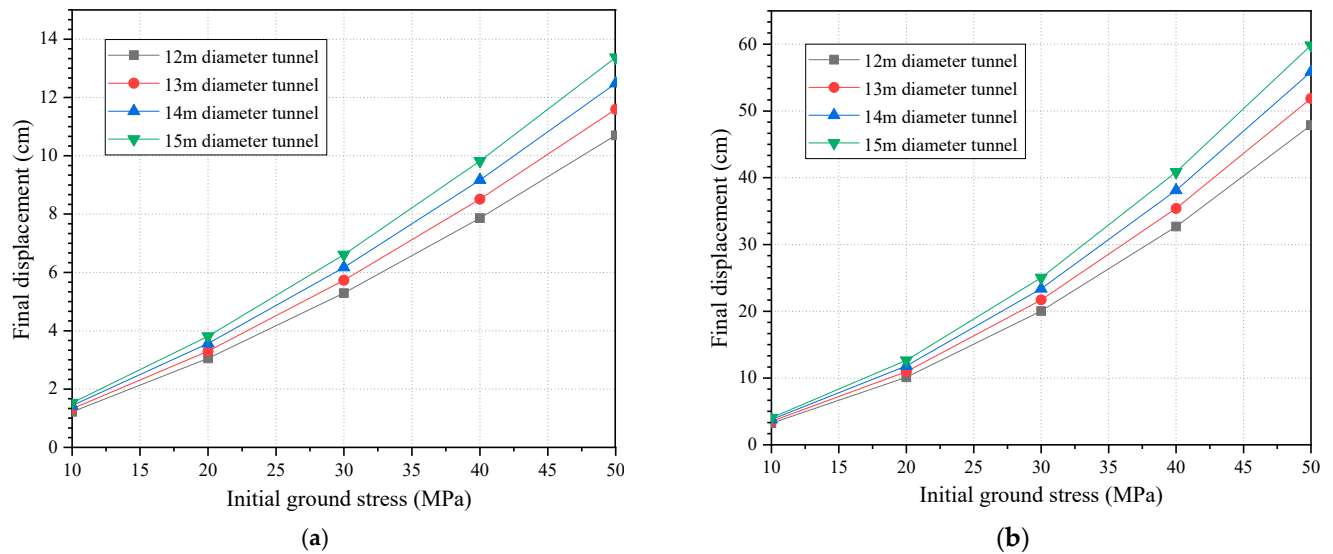


Figure 16. Final displacement curve around unsupported tunnel ($p_a = 1$ MPa). (a) Type III surrounding rock; (b) Type IV surrounding rock.

The limit displacement around the tunnel under the condition of Type IV surrounding rock was obviously greater than that of Type III surrounding rock. The larger the hole diameter, the greater the displacement. With the increase in in situ stress, the trend of displacement increases is more obvious.

According to the disclosed T_1 stratum (Type IV surrounding rock), it was known that the buried depth was 1550~1850 m, and the in situ stress was about 45 MPa. When the tunnel diameter was 13.4 m, the displacement around the tunnel was 70 cm without support. When the support resistance $p_a = 1$ MPa, it was 45 cm. When the support resistance

$p_a = 2$ MPa, it was 33 cm. Considering the hysteresis of the supporting effect, the reserved deformation should have been greater than the displacement when there was supporting resistance and less than the displacement around the tunnel when there was no supporting resistance. Considering the support resistance of 1 MPa, the reserved deformation range can be 45~70 cm. Considering the support resistance of 2 MPa, the reserved deformation range can be 33~70 cm.

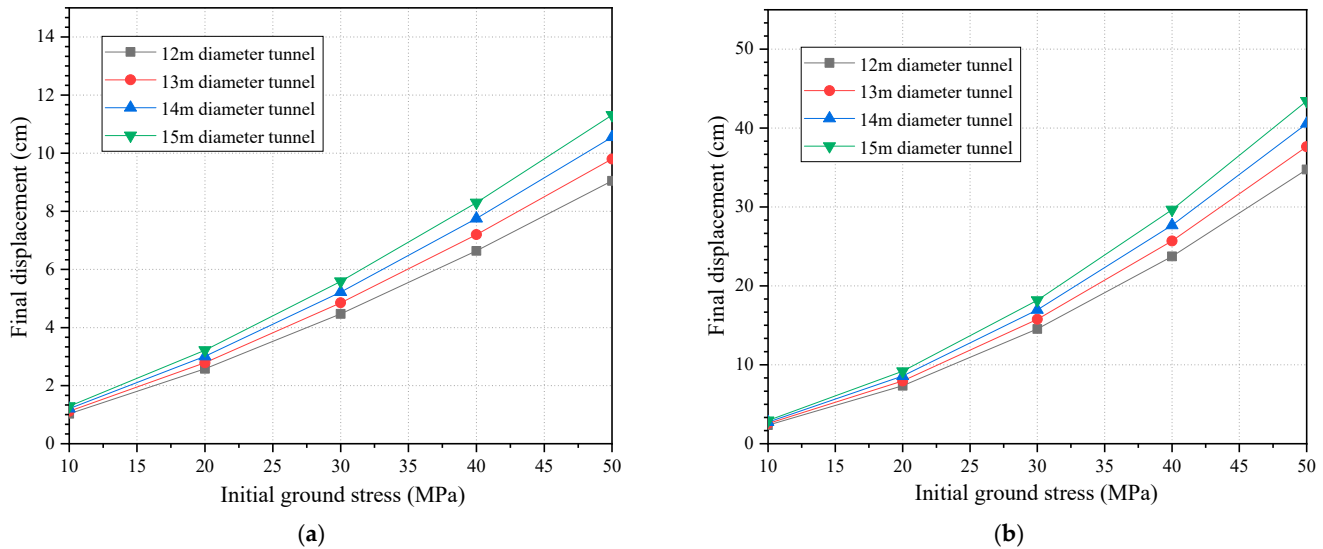


Figure 17. Final displacement curve around unsupported tunnel ($p_a = 2$ MPa). (a) Type III surrounding rock; (b) Type IV surrounding rock.

5.3. Numerical Calculations

The maximum deformation, which depended on the strength of the surrounding rock, the amount of in situ stress, the stiffness of the support, and the duration of the support, was intimately linked to the reserved deformation. This part used the limit displacement of the tunnel without support as a guide to determine the reserved deformation, taking into consideration the uncertainty of the supporting function.

The mechanical calculation parameters of the surrounding rock of the tunnel are also shown in Table 1. The deformation of the surrounding rock under 40 working conditions and under four conditions of 10 MPa, 20 MPa, 30 MPa, 40 MPa, and 50 MPa and cavern diameters of 12 m, 13 m, 14 m, 15 m in grade III and IV surrounding rock conditions were simulated. The calculation model and related boundary conditions and parameters were the same as in Section 4.2. The calculation results are shown in Figure 18.

It is evident that the surrounding rock grade has the greatest impact on the surrounding rock deformation. With the improvement in the surrounding rock grade, the integrity of the rock decreases and the development of cracks increases, which leads to a significant decrease in the strength and stiffness of the rock, which makes the surrounding rock more prone to deformation under the same stress conditions. The displacement of the surrounding rock increases by 5~10 times with each increase in the surrounding rock level. For example, the maximum deformation of Grade III surrounding rock is 12~17 cm, while the maximum deformation of Grade IV surrounding rock is 95~115 cm. This sharp increase in deformation not only increases the burden of the supporting structure but also may pose a threat to the overall safety of the project. In the relatively low stress range of 10~50 MPa, there is an approximate linear relationship between surrounding rock displacement and in situ stress. This means that with the gradual increase in in situ stress, the deformation of surrounding rock will also increase in proportion. However, when the local stress exceeds a certain critical value, this linear relationship may change, because the rock may enter a plastic or failure state at this time, resulting in a more complicated deformation mechanism. Although the effect of the cave diameter on the displacement of the adjacent rock is minor, it

cannot be overlooked. As a special geological structure in underground space, the existence of a karst cave will change the stress distribution and deformation mode of the surrounding rock mass. When the diameter of the cave increases, the stress concentration around the cave intensifies, which may lead to local rock mass destruction and a displacement increase. In addition, factors such as the nature of the filler in the cave and the relative position between the cave and the tunnel may also have some influence on the deformation of the surrounding rock. When comparing the theoretical calculation results with the actual situation, the simulation results are often too large, and the arch waist displacement is generally greater than the vault displacement. This deviation comes from many aspects: first, theoretical models are usually based on a series of simplifications and assumptions, and it is difficult to fully reflect the complexity and variability of actual projects; second, the uncertainty of field geological conditions, the disturbance in the construction process, and the error of monitoring data may also lead to the difference between theory and practice; finally, the arch waist position is more prone to large deformation because of its complex stress and relatively weak supporting conditions.

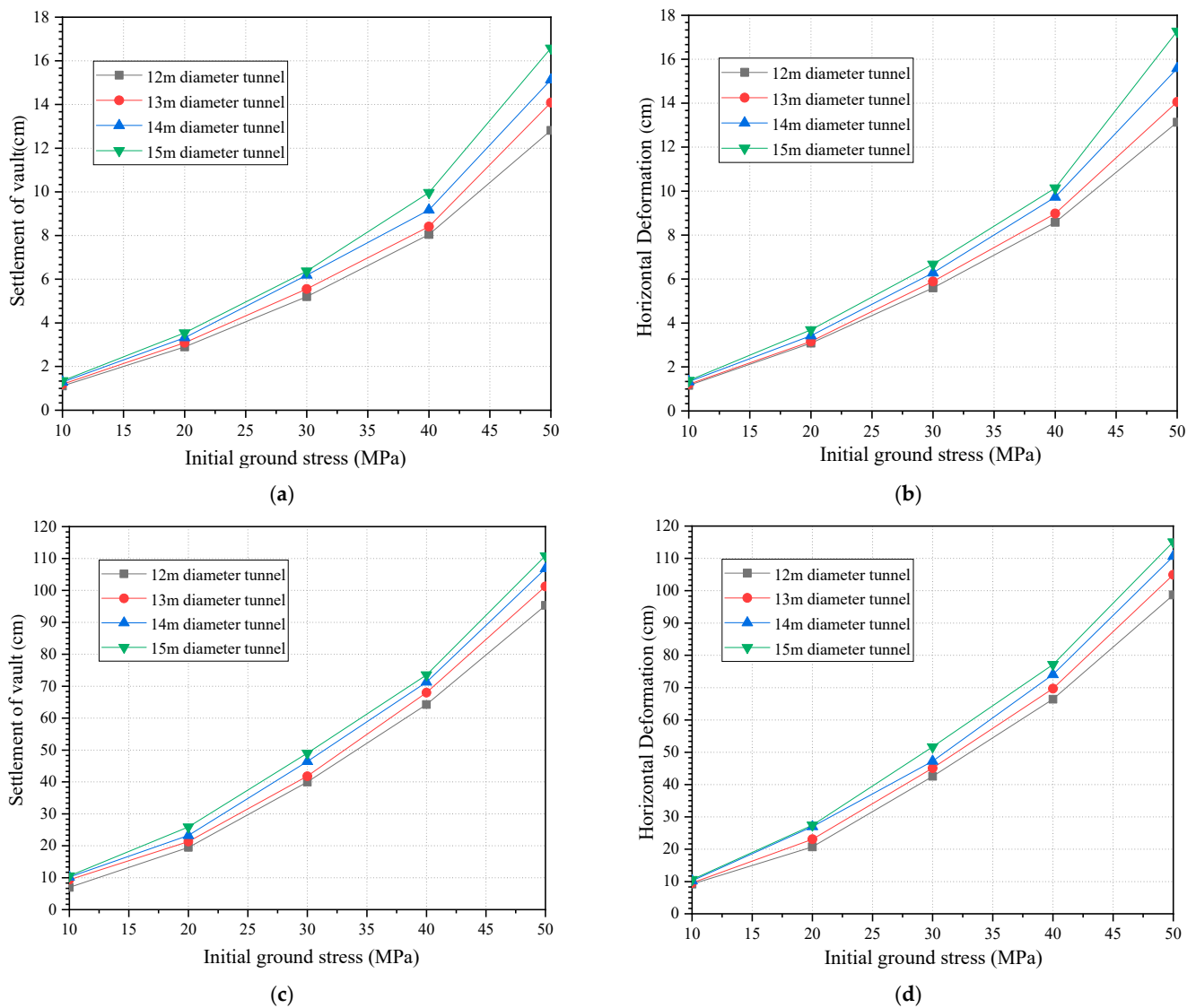


Figure 18. Displacement curve. (a) Settlement of Vault of Type III; (b) Horizontal Deformation of Type III; (c) Settlement of Vault of Type IV; (d) Horizontal Deformation of Type IV.

Based on the above calculation results, the reserved deformation of the tunnel can be estimated in a more detailed macro way. This estimation not only depends on the

specific surrounding rock grade, cave diameter, and in situ stress conditions but can also be combined with mathematical tools such as an interpolation method to accurately predict the maximum deformation under different conditions. According to the existing calculation results, including the surrounding rock deformation data under different surrounding rock grades, cave diameters, and in situ stresses, a multi-dimensional deformation prediction model is constructed. Check the corresponding calculation results and make predictions. It can effectively deal with continuously changing geological conditions and engineering parameters and improve the accuracy and reliability of reserved deformation estimation. When the in situ stress of the Class IV surrounding rock section is 45 MPa and the tunnel diameter is 13 m, these specific conditions can be input into the prediction model. The maximum deformation of the vault is 82 cm and the maximum horizontal displacement of the arch waist is 84 cm. This shows that under complex geological conditions, the actual deformation may significantly exceed the theoretical calculation results based on simplified assumptions. To confirm the validity of the prediction results, we compare and analyze the simulation results against the theoretical calculation values. As can be seen in Table 2, the simulation results (such as vault 82 cm and arch waist 84 cm) have a higher assurance rate than the theoretical calculation value of 70 cm, which further proves the importance and application value of numerical simulation in complex geological engineering.

6. Conclusions

In this paper, the deformation characteristics of the diversion tunnel of Jinping II Hydropower Station are studied. Based on field statistics, theoretical calculation, and numerical simulation, considering the size, in situ stress, and grade of the surrounding rock, the reasonable reserved deformation of the deep soft rock tunnel is studied.

- (1) The initial support deformation of the diversion tunnel is serious, although it does not directly cause large-scale cracking of the sprayed concrete layer, but its manifestations—the emergence of a cave wall bulge and local “prick” shape—fully show that the stability of the surrounding rock has been significantly affected. This deformation mode not only increases the stress burden of the supporting structure but also poses a threat to the subsequent construction safety and long-term stability of the tunnel. The intrusion of the pure green schist karst cave section into the design lining space is as high as 21.7% to 176.7%, which leads to the deformation of tunnel surrounding rock accounting for 20 to 60 cm of the design lining gap thickness. This intrusion and deformation not only reduce the effective thickness of the lining but also affect the interaction between the lining and surrounding rock, reducing the bearing capacity of the whole structure.
- (2) The tunnel diameter, surrounding rock grade, in situ stress, and other factors will affect the tunnel deformation. On the premise of the reasonable selection of calculation parameters, the numerical calculation method is closer to the actual situation and can be used as the calculation method of reserved deformation. Various factors influence the reserved deformation, including the surrounding rock grade (lithology), in situ stress, and cave diameter.
- (3) Considering the actual situation of the chlorite schist section at the west end of the Jinping diversion tunnel and the influence of support, in order to ensure the construction safety and structural stability, it is suggested to set the reserved deformation space of the tunnel as a flexible interval of 30 cm to 60 cm. In view of the direct influence of the distribution of the chlorite schist section on the deformation allowance, this paper puts forward some suggestions on optimizing the tunnel diameter design: adjusting the original planned diameter range from 13.4 m to 13.8 m to 14.6 m. Specifically, when the tunnel passes through many sections of chlorite schist, the reserved deformation should be appropriately increased to the upper limit of the section or higher to fully absorb the deformation of the surrounding rock. On the other hand, if the chlorite schist section accounts for a small proportion, the reserved deformation can

be controlled near the lower limit of the section to realize a more economical and reasonable tunnel size design.

Author Contributions: Z.Y. proposed the research plan and framework ideas for this article and completed the writing of the original draft; P.L. provided financial support for the research of the project and investigated the geological conditions and distribution of buildings and structures within the study area; B.W. carried out the numerical simulation after receiving the processed data and analyzed and verified the prediction results; Y.Z. processed the data collected during the construction and optimized the readability of the chart; H.Z. optimized the organizational structure of the article and offered useful suggestions for the preparation and writing of the paper. All authors have read and agreed to the published version of the manuscript.

Funding: The study was supported by the High-Speed Railway and Natural Science United Foundation of China (U1934213) and the General Program of the National Natural Science Foundation of China (51878572).

Institutional Review Board Statement: Not applicable.

Informed Consent Statement: Not applicable.

Data Availability Statement: The original contributions presented in the study are included in the article, further inquiries can be directed to the corresponding author.

Acknowledgments: We also highly appreciate the data collection and processing work of China Railway Eryuan Engineering Group Co., Ltd. and the Key Laboratory of Transportation Tunnel Engineering of Southwest Jiaotong University. Finally, the authors would like to thank the reviewers for their useful comments and the editors for improving the manuscript.

Conflicts of Interest: Authors Zhen Yang and Peisi Liu were employed by the company Gansu Tianlong Railway Co., Ltd. and China Railway Eryuan Engineering Group Co., Ltd. The remaining authors declare that the research was conducted in the absence of any commercial or financial relationships that could be construed as a potential conflict of interest.

References

1. Wang, Y.; Ling, K.; Yang, Y.Y.; Zhang, Z.Q.; Xing, A.Q.; He, M.C.; Liu, D.Q. Experimental study on impact rockburst of surrounding rock in deep elliptical caverns. *Chin. J. Rock Mech. Eng.* **2021**, *40*, 2214–2228.
2. Cai, W.; Zhu, H.; Liang, W.; Vu, B.; Wu, W. Physical and Numerical Investigation on Nonlinear Mechanical Properties of Deep-Buried Rock Tunnel Excavation Unloading under Complicated Ground Stresses. *Tunn. Undergr. Space Technol.* **2023**, *138*, 105197. [[CrossRef](#)]
3. Zhang, J.; Cui, Z.; Sheng, Q.; Zhao, W.; Song, L. Experimental Study on the Effect of Flexible Joints of a Deep-Buried Tunnel across an Active Fault under High in-Situ Stress Conditions. *Undergr. Space* **2024**, *19*, 189–207. [[CrossRef](#)]
4. Bai, C.H.; Xue, Y.G.; Qiu, D.H.; Su, M.X.; Ma, X.M.; Liu, H.T. Analysis of factors affecting the deformation of soft rock tunnels by data envelopment analysis and a risk assessment model. *Tunn. Undergr. Space Technol.* **2021**, *116*, 104111. [[CrossRef](#)]
5. Zhang, C.Q.; Cui, G.J.; Zhang, Y.; Zhou, H.; Liu, N.; Huang, S.L. Squeezing deformation control during bench excavation for the Jinping deep soft-rock tunnel. *Eng. Fail. Anal.* **2020**, *116*, 104761. [[CrossRef](#)]
6. Bao, H.; Liu, C.; Liang, N.; Lan, H.; Yan, C.; Xu, X. Analysis of Large Deformation of Deep-Buried Brittle Rock Tunnel in Strong Tectonic Active Area Based on Macro and Microcrack Evolution. *Eng. Fail. Anal.* **2022**, *138*, 106351. [[CrossRef](#)]
7. Sun, Z.; Zhang, D.; Li, M.; Guo, F. Large Deformation Characteristics and the Countermeasures of a Deep-Buried Tunnel in Layered Shale under Groundwater. *Tunn. Undergr. Space Technol.* **2024**, *144*, 105575. [[CrossRef](#)]
8. Bian, K.; Liu, J.; Liu, Z.P.; Liu, S.G.; Ai, F.; Zheng, X.Q.; Ni, S.H.; Zhang, W. Mechanisms of large deformation in soft rock tunnels: A case study of Huangjiazhai Tunnel. *Bull. Eng. Geol. Environ.* **2019**, *78*, 431–444. [[CrossRef](#)]
9. Cao, C.Y.; Shi, C.H.; Le, M.F.; Yang, W.C.; Liu, J.W. Squeezing failure of tunnels: A case study. *Tunn. Undergr. Space Technol.* **2018**, *77*, 188–203. [[CrossRef](#)]
10. Chen, Z.Q.; He, C.; Xu, G.W.; Ma, G.Y.; Yang, W.B. Supporting mechanism and mechanical behavior of a double primary support method for tunnels in broken phyllite under high geo-stress: A case study. *Bull. Eng. Geol. Environ.* **2019**, *78*, 5253–5267. [[CrossRef](#)]
11. Liu, W.W.; Chen, J.X.; Luo, Y.B.; Chen, L.J.; Shi, Z.; Wu, Y.F. Deformation behaviors and mechanical mechanisms of double primary linings for large-span tunnels in squeezing rock: A case study. *Rock Mech. Rock Eng.* **2021**, *54*, 2291–2310. [[CrossRef](#)]
12. Zhang, J.R.; Ma, K.M.; Fang, Q.B.; Kong, C.; Jiao, K.J. Study on Reasonable Tunnel Types of Steeply Dipping Slate Tunnels with High Geostress Based on Deformation Characteristics of Layered Surrounding Rock. *China J. Highw. Transp.* **2020**, *33*, 215.
13. Xu, F.; Li, S.C.; Zhang, Q.Q.; Li, L.P.; Shi, S.S.; Zhang, Q. A new type support structure introduction and its contrast study with traditional support structure used in tunnel construction. *Tunn. Undergr. Space Technol.* **2017**, *63*, 171–182. [[CrossRef](#)]

14. Qiu, W.G.; Lu, F.; Wang, G.; Huang, G.; Zhang, H.J.; Zhang, Z.Y.; Gong, C. Evaluation of mechanical performance and optimization design for lattice girders. *Tunn. Undergr. Space Technol.* **2019**, *87*, 100–111. [[CrossRef](#)]
15. Wang, Q.; Jiang, B.; Pan, R.; Li, S.C.; He, M.C.; Sun, H.B.; Qin, Q.; Yu, H.C.; Luan, Y.C. Failure mechanism of surrounding rock with high stress and confined concrete support system. *Int. J. Rock Mech. Min. Sci.* **2018**, *102*, 89–100. [[CrossRef](#)]
16. Qiu, W.; Wang, G.; Gong, L.; Shen, Z.; Li, C.; Dang, J. Research and application of resistance-limiting and energy-dissipating support in large deformation tunnel. *Chin. J. Rock Mech. Eng.* **2018**, *37*, 1786–1795. (In Chinese)
17. Wang, F.N.; Guo, Z.B.; Qiao, X.B.; Fan, J.Y.; Li, W.; Mi, M.; Tao, Z.G.; He, M.C. Large deformation mechanism of thin-layered carbonaceous slate and energy coupling support technology of NPR anchor cable in Minxian Tunnel: A case study. *Tunn. Undergr. Space Technol.* **2021**, *117*, 104151. [[CrossRef](#)]
18. Sun, X.M.; Zhao, C.W.; Tao, Z.G.; Kang, H.W.; He, M.C. Failure mechanism and control technology of large deformation for Muzhailing Tunnel in stratified rock masses. *Bull. Eng. Geol. Environ.* **2021**, *80*, 4731–4750. [[CrossRef](#)]
19. Chen, L.J.; Chen, J.X.; Luo, Y.B.; Liu, W.W.; Wang, C.W. Deformation Law and Reasonable Reserved Deformation of Deep Large-span Chlorite Schist Tunnel. *China J. Highw. Transp.* **2021**, *34*, 147. (In Chinese)
20. Ding, Y.Z.; Tan, Z.S.; Ma, D. Study on large deformation characteristics and control measures of soft rock tunnel in fault zone with high geostress. *China Civ. Eng. J.* **2017**, *50*, 129–134. (In Chinese)
21. Yang, F.J.; Zhang, C.Q.; Zhou, H.; Liu, N.; Zhang, Y.; Azhar, M.U.; Dai, F. The long-term safety of a deeply buried soft rock tunnel lining under inside-to-outside seepage conditions. *Tunn. Undergr. Space Technol.* **2017**, *67*, 132–146. [[CrossRef](#)]
22. Zhou, H.; Zhang, C.Q.; Li, Z.; Hu, D.W.; Hou, J. Analysis of mechanical behavior of soft rocks and stability control in deep tunnels. *J. Rock Mech. Geotech. Eng.* **2014**, *6*, 219–226. [[CrossRef](#)]
23. *JTG3370.1-2018*; Specifications for Design of Highway Tunnels Section 1 Civil Engineering. China Communications Press: Beijing, China, 2018.
24. *TB 10003-2016*; Code for Design of Railway Tunnel. China Railway Publishing House: Beijing, China, 2016.
25. Liu, Q.F.; Liu, Q.Z. Experimental Research on Image Acquisition Method of Tunnel Lining Cracks Based on Line-scanning Digital Camera. *Mod. Tunn. Technol.* **2020**, *1*, 142–147+161. (In Chinese)
26. Zhao, H.L.; Qiu, W.G.; Qi, X.X. Optimization of Reserved Tunnel Deformation Based on 3D Laser Scanning Technology. *Tunn. Constr.* **2020**, *40*, 1607–1614. (In Chinese)
27. Li, M.; Mao, X.B.; Yu, Y.L.; Li, K.; Ma, C.; Peng, Y. Stress and deformation analysis on deep surrounding rock at different time stages and its application. *Int. J. Min. Sci. Technol.* **2012**, *22*, 301–306. [[CrossRef](#)]
28. Luo, Y.B.; Chen, J.X.; Gao, S.T.; Deng, X.H.; Diao, P.S. Stability analysis of super-large-section tunnel in loess ground considering water infiltration caused by irrigation. *Environ. Earth Sci.* **2017**, *76*, 763. [[CrossRef](#)]
29. Cui, G.Y.; Ma, J.F.; Wang, D.Y. A large 3D laboratory test on the deformation characteristic of shallow loess tunnel under different plastic states. *Bull. Eng. Geol. Environ.* **2021**, *80*, 7577–7590. [[CrossRef](#)]
30. Wang, D.Y.; Yuan, J.X.; Zhu, Y.Q.; Liu, J.; Wang, H.F. Model test study of deformation characteristics and reasonable reserved deformation of shallow-buried loess tunnel with hard-flow plastic. *Rock Soil Mech.* **2019**, *40*, 3813–3822. (In Chinese)
31. Hoek, E.; Associates, G.; Cannada, V. Strength of jointed rock masses. *Geotechnique* **1983**, *33*, 187–223. [[CrossRef](#)]
32. Saroglou, H.; Tsiambaos, G. A modified Hoek–Brown failure criterion for anisotropic intact rock. *J. Rock Mech. Min. Sci.* **2008**, *45*, 223–234. [[CrossRef](#)]

Disclaimer/Publisher’s Note: The statements, opinions and data contained in all publications are solely those of the individual author(s) and contributor(s) and not of MDPI and/or the editor(s). MDPI and/or the editor(s) disclaim responsibility for any injury to people or property resulting from any ideas, methods, instructions or products referred to in the content.